Supplementary figures

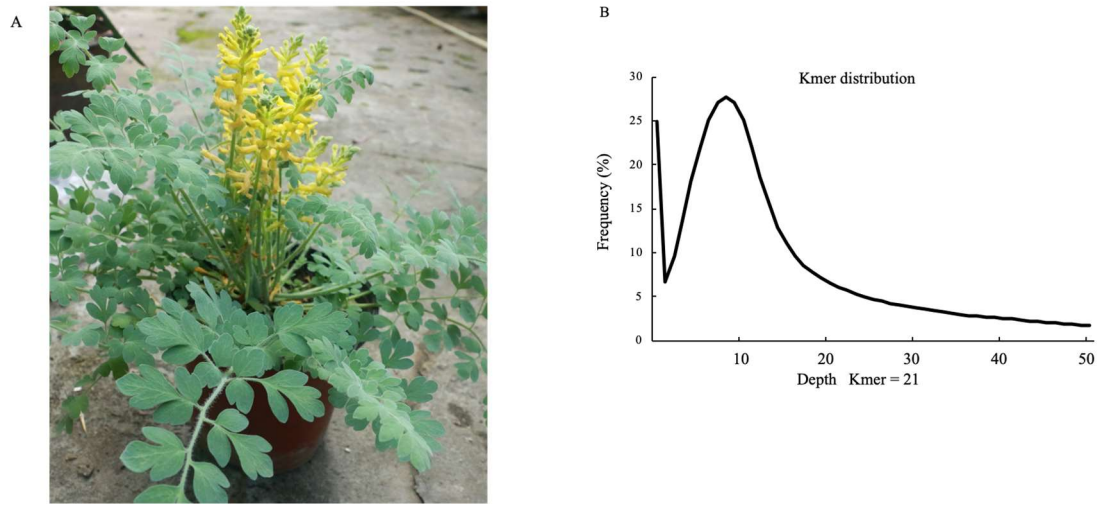

Figure S1. The morphology and genome survey of *C. tomentella*. The genome survey was performed using 21 *k*-mer distribution from Illumina short reads of *C. tomentella*.

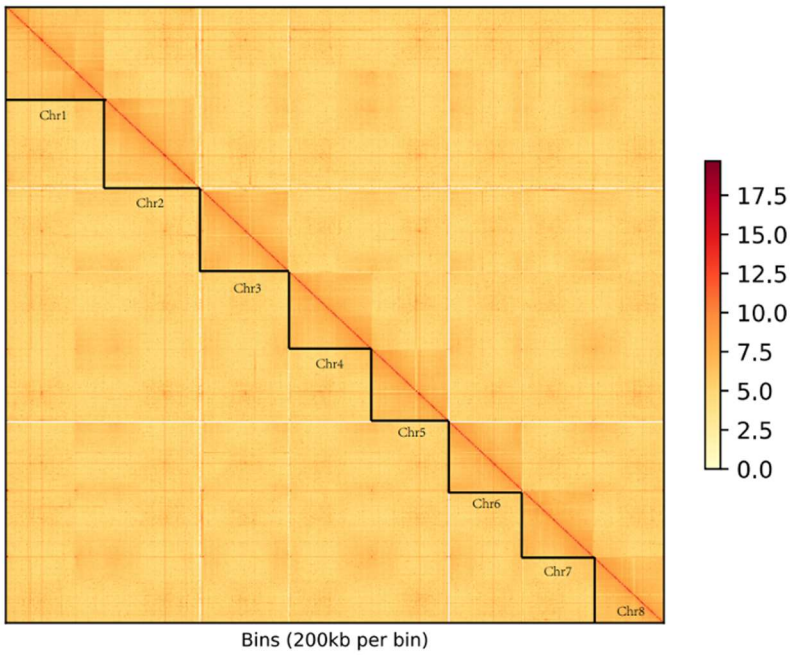

Figure S2. Hi-C intra-chromosomal contact map for the genome assembly (2n=16). The intensity of each pixel indicates the number of Hi-C links of 200 kb resolution in the chromosomes.

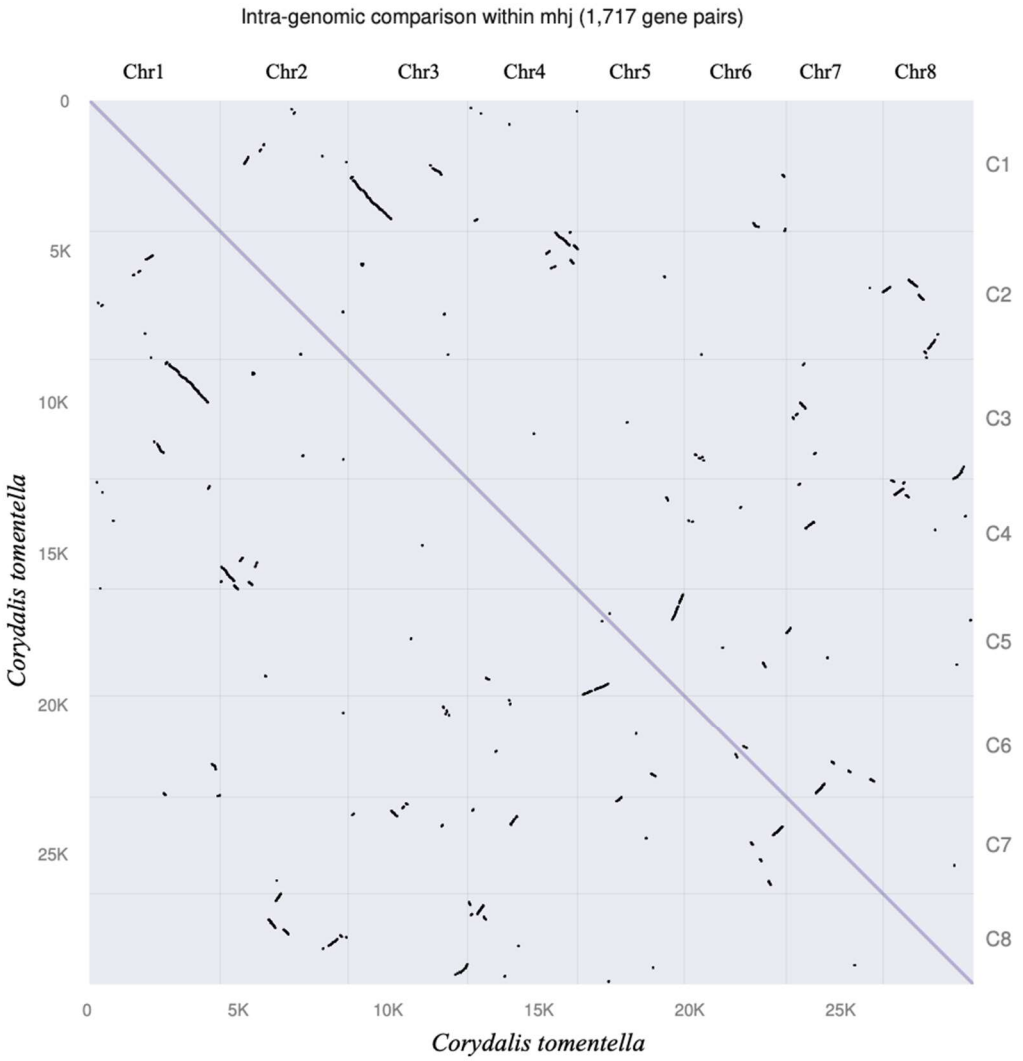

Figure S3. Dot plot of paralogous blocks in *C. tomentella* shows the potential whole genome duplication event.

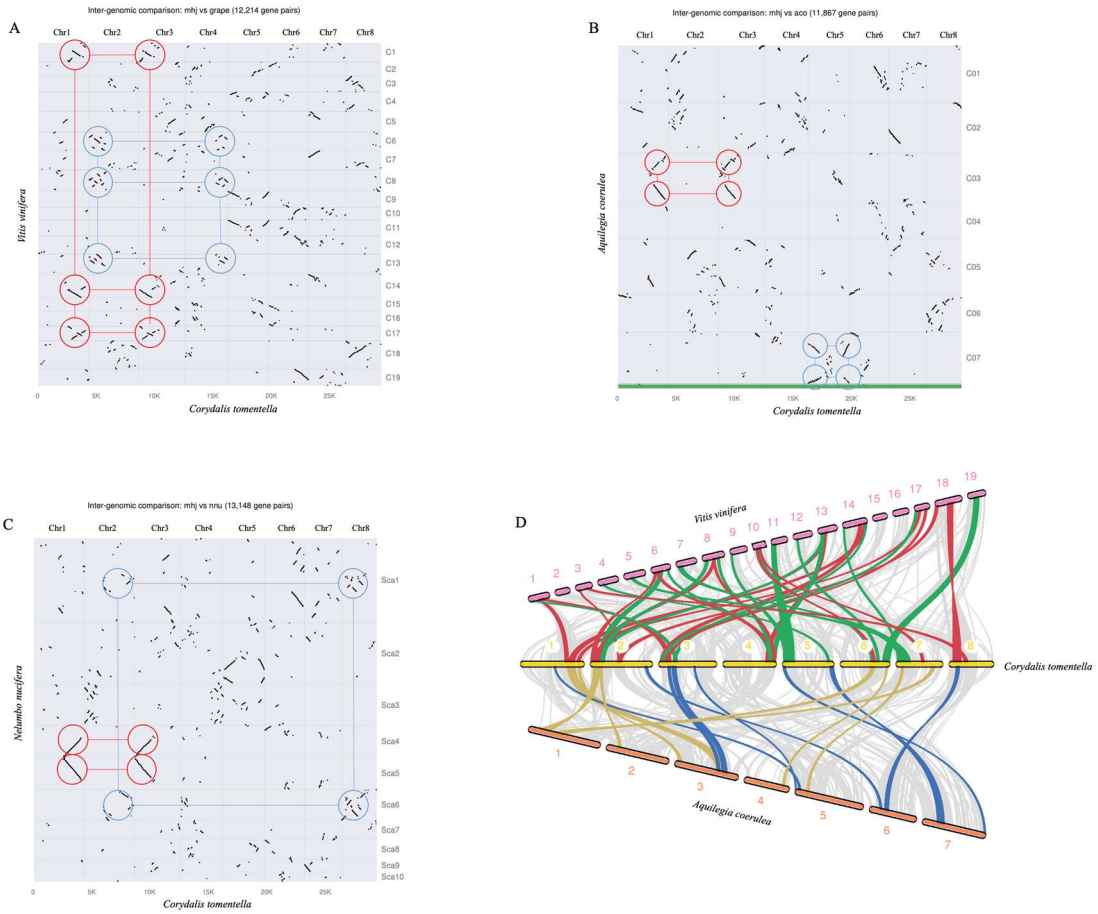

Figure S4. Synteny analysis between the *C. tomentella* and other eudicot genomes. Dot plots showed the syntenic orthologs between *C. tomentella* and *V. vinifera* (A), between *C. tomentella* and *A. coerulea* (B), and between *C. tomentella* and *N. nucifera* (C). The red and blue circles highlight several duplication regions. D. Macrosynteny between *C. tomentella* and *V. vinifera*, and between *C. tomentella* and *A. coerulea* chromosomes. Red lines highlight three duplication blocks in *V. vinifera* genome per corresponding *C. tomentella* region. Green lines represent two duplication blocks in *C. tomentella* genome per corresponding *V. vinifera* region. Yellow lines highlight two duplication blocks in *C. tomentella* genome per corresponding *A. coerulea* region. Blue lines represent two duplication blocks in *A. coerulea* genome per corresponding *C. tomentella* region.

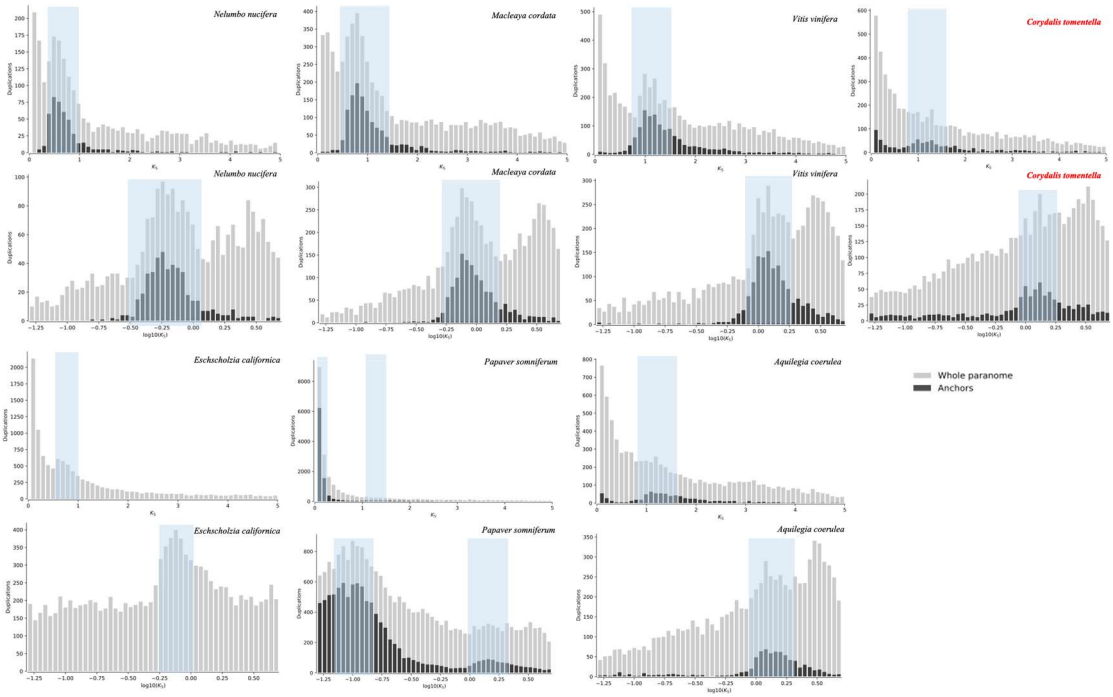

Figure S5. K_S distributions of whole paralogs (grey bars) and anchor-pair paralogs (black bars) for *Vitis vinifera* and six sister lineages to core eudicots (*Nelumbo nucifera*, *Aquilegia coerulea*, *Corydalis tomentella*, *Macleaya cordata*, *Papaver somniferum*, and *Eschscholzia californica*). The blue rectangles highlight the K_S peak ranges, represented the whole genome duplication events.

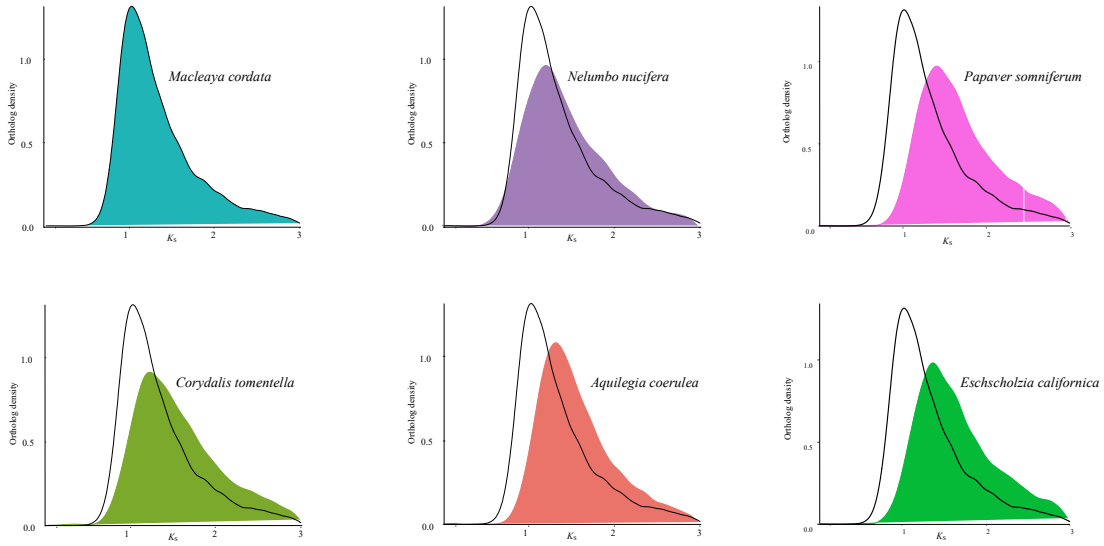

Figure S6. The kernel density estimation (KDE) of the orthologous K_S distributions between *V. vinifera* and six sister lineages to core eudicots. The KDE of black line in each plot is the orthologous K_S distribution between *V. vinifera* and *M. cordata*. The KDEs of different colors are the orthologous K_S distributions between *V. vinifera* and each species.

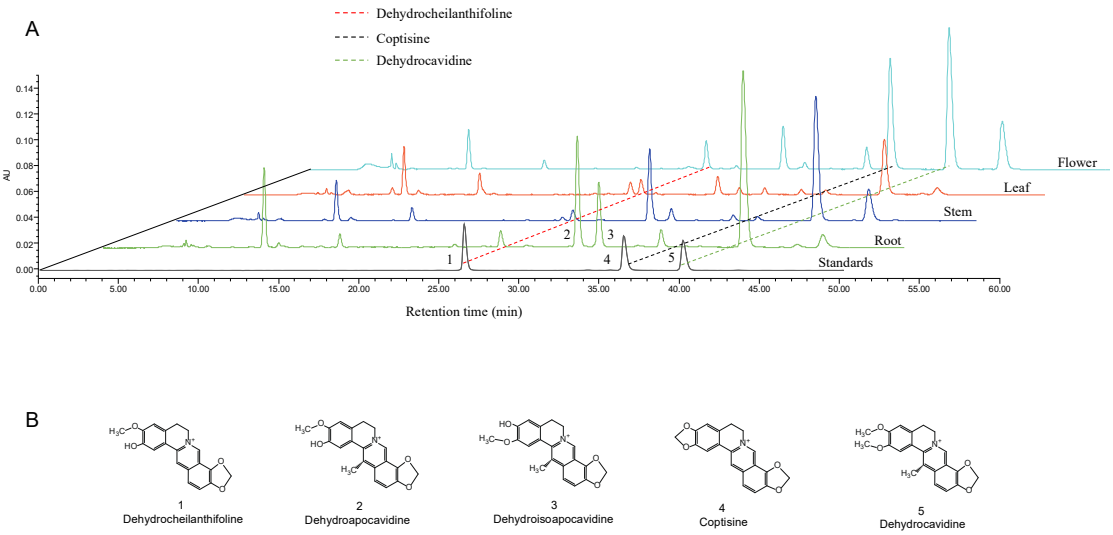

Figure S7. A: HPLC analysis of BIAs in *C. tomentella* at different tissues, including root, stem, leaf and flower. Dehydrocheilanthifoline (1: 25.74 min); Dehydroapocavidine (2: 30.11 min); Dehydroisoapocavidine (3: 32.46 min); Coptisine (4: 36.33 min); Dehydrocavidine (5: 40.01 min). B: The chemical structure of enriched BIAs (1-5) in *C. tomentella*. The detection wavelength is 347nm. The standards of dehydrocheilanthifoline (1), coptisine (4), and dehydrocavidine (5) were purchased from Chengdu Biopurify Phytochemicals Ltd. However, we could not get the standards of dehydroapocavidine (2) and dehydroisoapocavidine (3). Therefore, we identified the chemical structures of dehydroapocavidine (2) and dehydroisoapocavidine (3) via the extraction, separation, and purification of these BIAs from *Corydalis*. The results are presented in Figure S8 and S9.

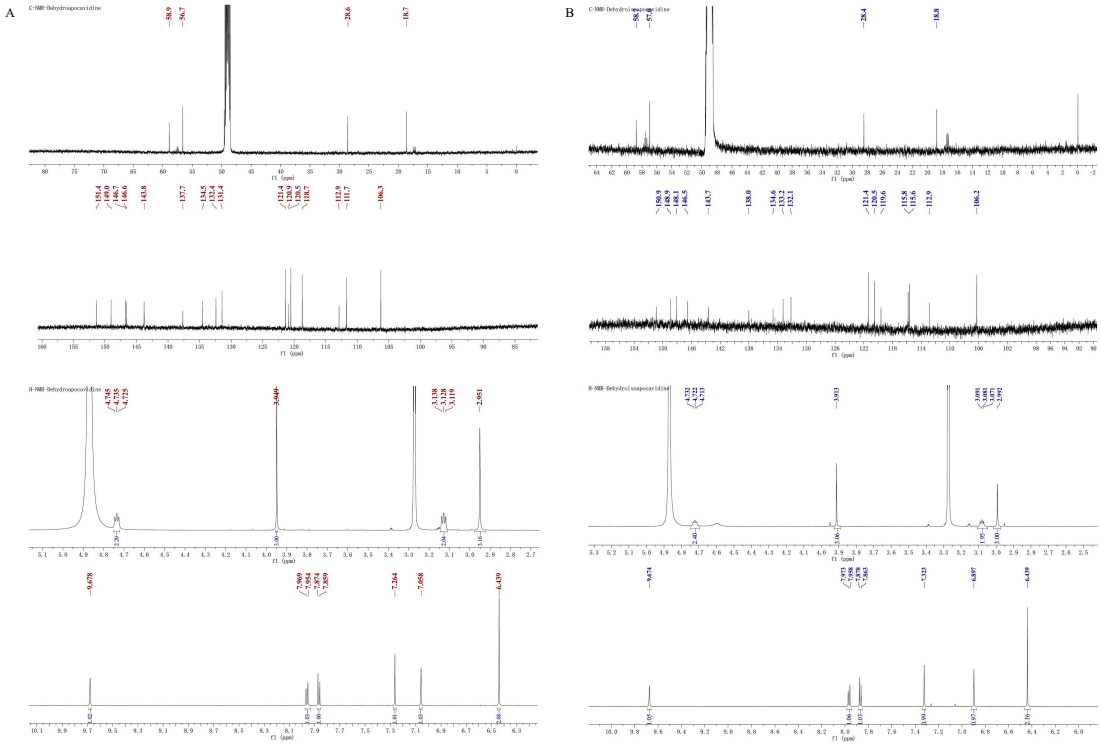

Figure S8. ^{1}H NMR and ^{13}C NMR spectra of dehydroapocavidine (A) and dehydroisoapocavidine (B) in Methanol-D4 using Bruker 600MHz.

A

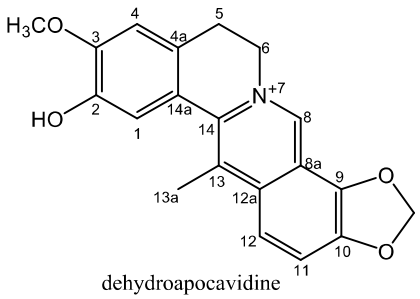

dehydroapocavidine

Carbon	^{13}C	^{1}H
1	112.9	7.264(1H, s)
2	151.4	-
3	149	-
3-OCH3	58.9	3.949(3H, s)
4	111.7	7.058(1H, s)
4a	137.7	
5	28.6	3.128(2H, t, *J*=6.0)
6	56.7	4.735(2H, t, *J*=6.0)
8	143.8	9.678(1H, s)
8a	134.5	-
9	146.7	-
10	146.6	-
9, 10-OCH2O-	106.3	6.439(2H, s)
11	118.7	7.87(1H, d, *J*=9.0)
12	121.4	7.96(1H, d, *J*=9.0)
12a	132.4	-
13	120.9	-
13a	18.7	2.951(3H, s)
14	131.4	-
14a	120.5	-

B

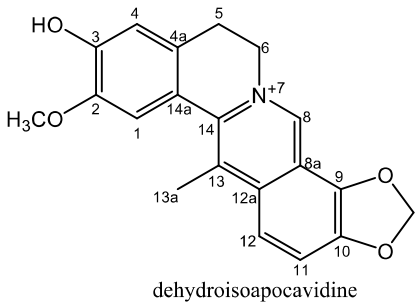

dehydroisoapocavidine

Carbon	^{13}C	^{1}H
1	115.6	7.323(1H, s)
2	148.9	-
3	150.9	-
3-OCH3	58.7	3.913(3H, s)
4	112.9	6.897(1H, s)
4a	138	
5	28.4	3.081(2H, t, J=6.0)
6	57	4.722(2H, t, J=6.0)
8	143.7	9.674(1H, s)
8a	134.6	-
9	148.1	-
10	146.5	-
9, 10-OCH2O-	106.2	6.439(2H, s)
11	115.8	7.87(1H, d, J=9.0)
12	121.4	7.96(1H, d, J=9.0)
12a	133.2	-
13	120.5	-
13a	18.58	2.992(3H, s)
14	132.1	-
14a	119.6	-

Figure S9. The identification of chemical structures of dehydroapocavidine (A) and dehydroisoapocavidine (B) based on the ^{1}H NMR and ^{13}C NMR spectra.

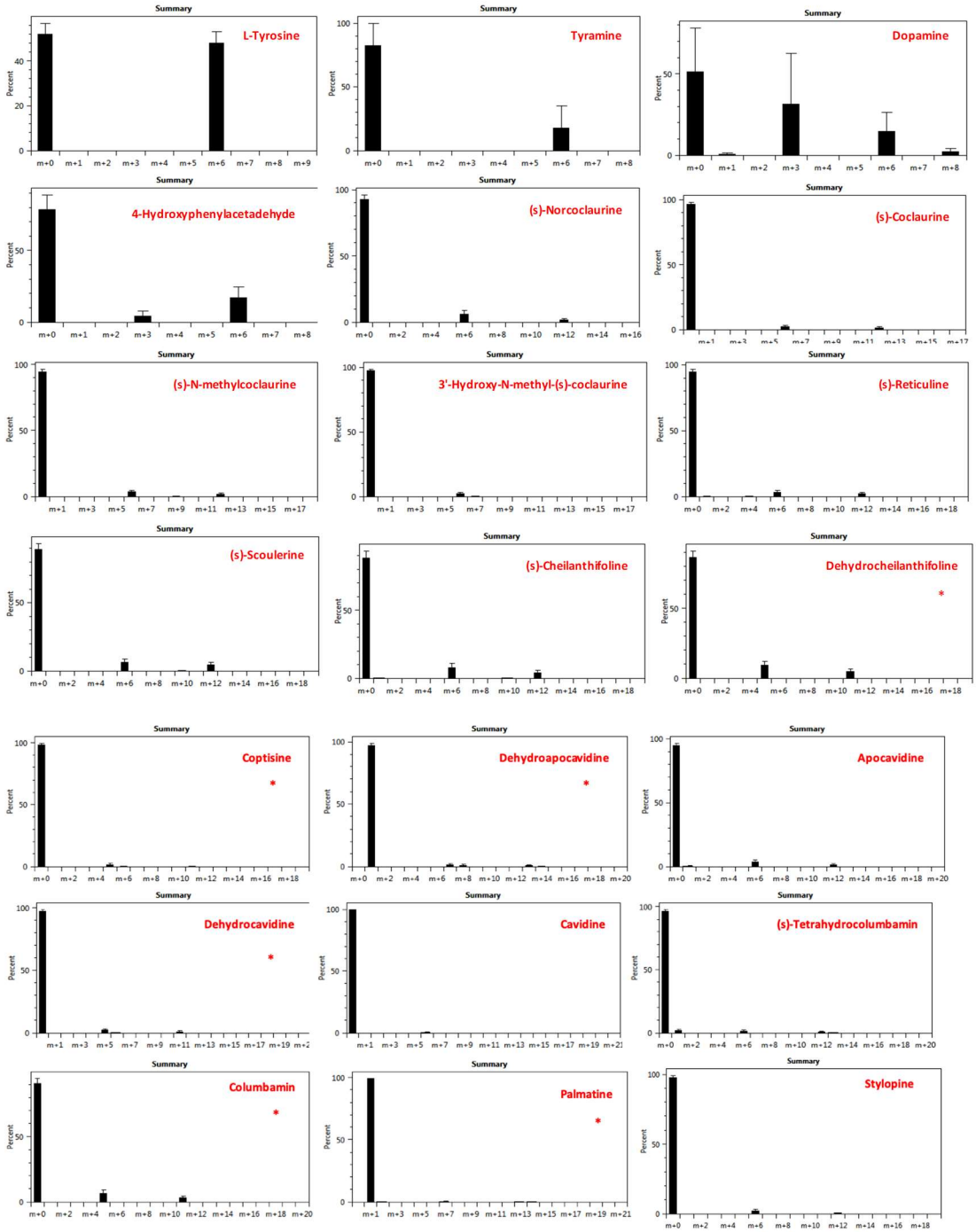

Figure S10. The proportion of labeled and unlabeled BIA compounds in the study of isotopic tracer. Among them, columbamine, palmatine, dehydroapocavidine, dehydrocheilanthifoline, coptisine, and dehydrocavidine are positively charged, and these compounds directly form positive ions in mass spectrometry without combining protons. However, the compounds were defaulted to add a proton to form the positive ions using the isotope data analysis software. Therefore, the molecular weights (MWs) of these labeled compounds, which are marked in red stars in the Figure, are 1 Da less that the real MWs. There are M+3 ions for dopamine and 4-hydroxyphenylacetadehyde detected after $^{13}C_6$ (benzene-ring)-labeled tyrosine feeding. However, there are not M+3 or M+9 ions

detected for the downstream BIAs, therefore, the observation of M+3 ions for these two compounds might not be resulted from the cleavage of the benzene-ring with $^{13}C_6$ label. In addition, these two compounds are high polarity, small molecular wights, bad chromatographic peak shapes. Therefore, we speculated that the M+3 or M+9 ions are not originated from the labeled tyrosine, but resulted from the interference of complex compounds.

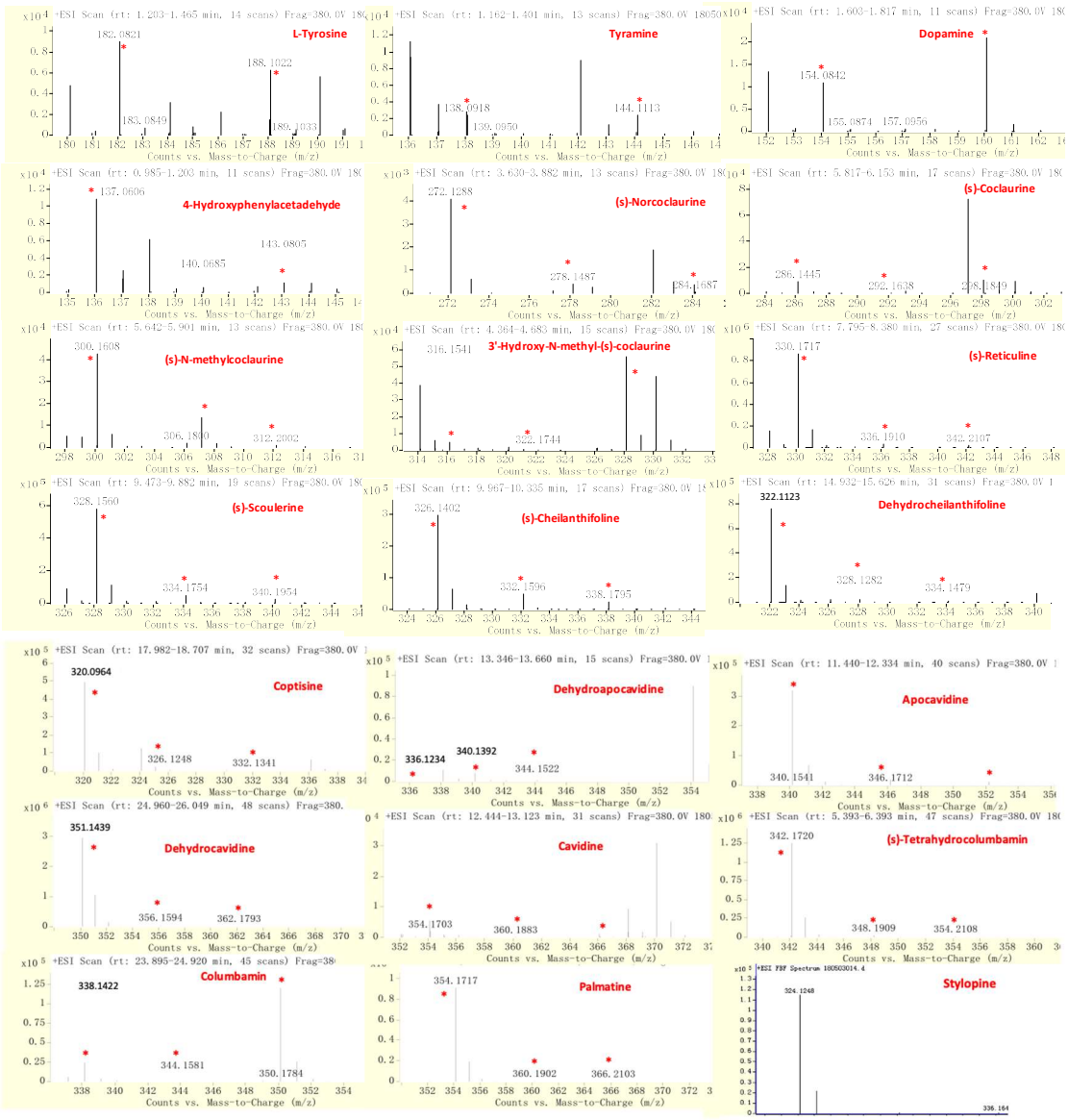

Figure S11. HRMS (High resolution mass spectrometry) analysis of detected BIA compounds in *C. tomentella*.

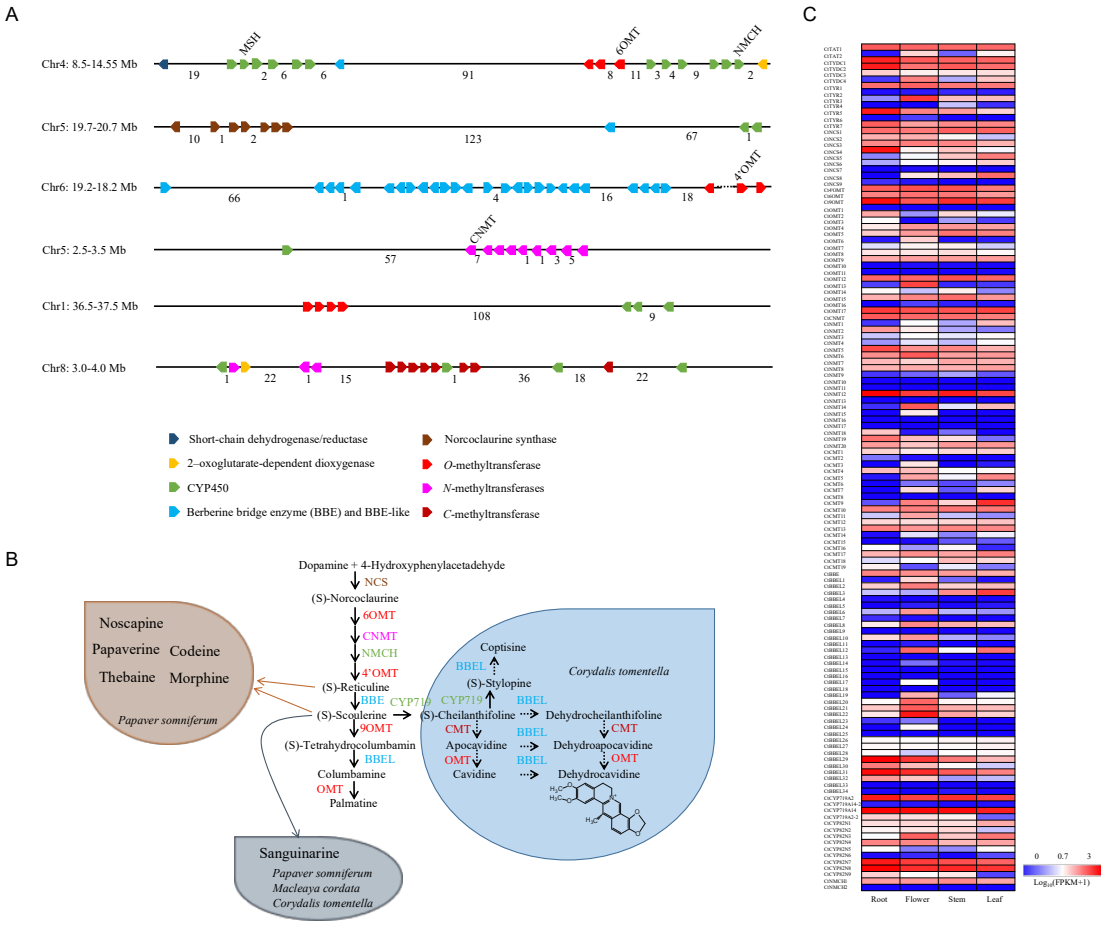

Figure S12. Gene cluster and gene expression analysis related to BIA biosynthesis in *C. tomentella*. A. Identification of gene cluster and tandem duplications of BIA biosynthetic genes in *C. tomentella* genome regions. The various genes were shown in different colors. B. The species-conserved and -specific biosynthetic pathway of BIAs in *P. somniferum*, *C. tomentella* and *M. cordata*. C. Gene expression patterns related to BIA biosynthetic genes from various organs of *C. tomentella*. The heatmap of gene expression values was calculated by $\log_{10}$(FPKM+1).

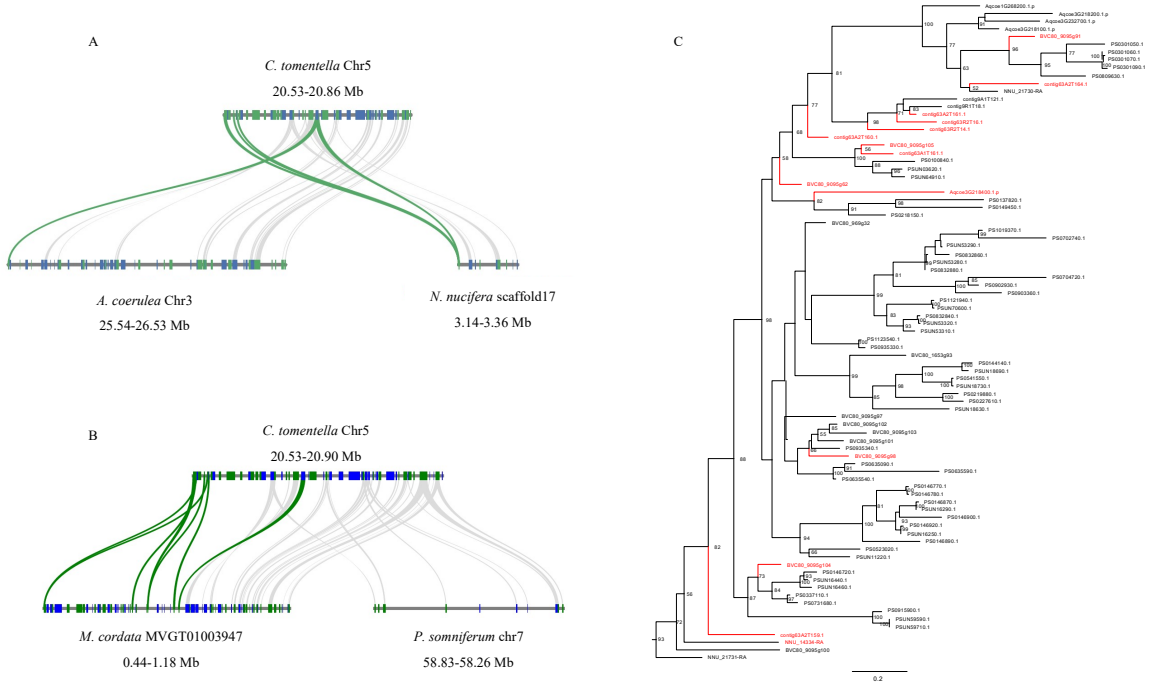

Figure S13. Evolutional analysis of NCS gene clusters among *A. coerulea* (AqcoeXGXXXXXX), *C. tomentella* (contigXXXXXX), *M. cordata* (BVC80_XXXXXXX), *P. somniferum* (PSXXXXXXX), and *N. nucifera* (NNU_XXXXX) genomes. A, Syntenic analysis of NCS genes in *C. tomentella*, *A. coerulea*, and *N. nucifera*. B, Syntenic analysis of NCS genes in *C. tomentella*, *M. cordata*, and *P. somniferum*. C, Maximum likelihood tree of NCS genes from candidate species. The red branches represented the NCS genes localized in the syntenic blocks.

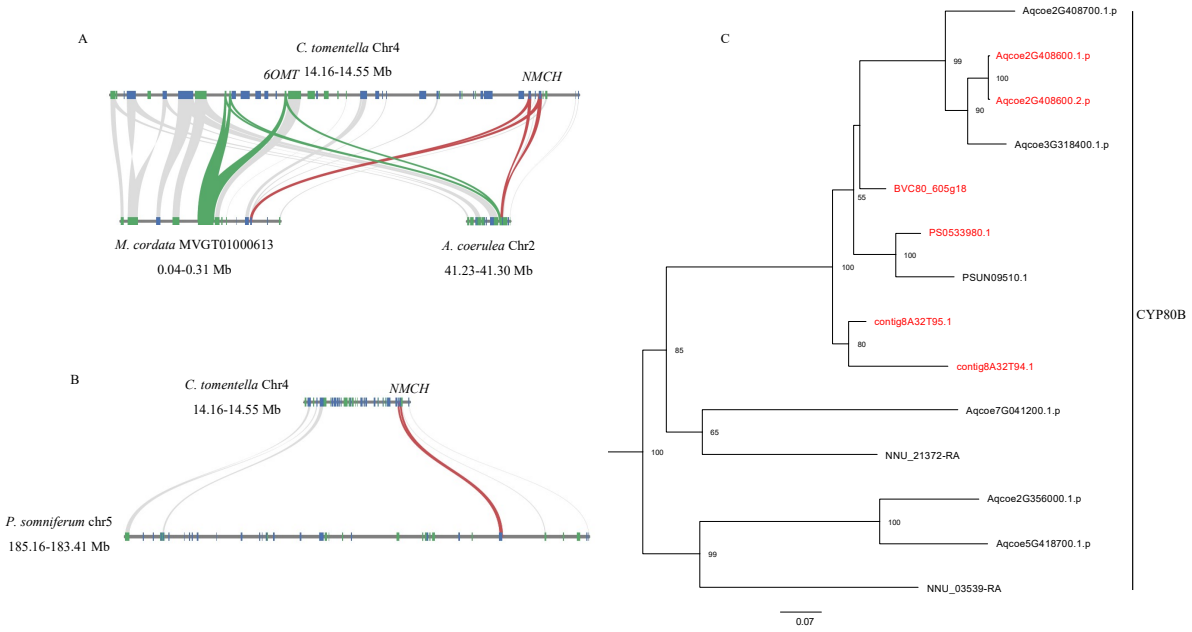

Figure S14. Evolutional analysis of 6OMT and NMCH genes among *A. coerulea* (AqcoeXGXXXXXX), *C. tomentella* (contigXXXXXX), *M. cordata* (BVC80_XXXXXXX), *P. somniferum* (PSXXXXXXX), and *N. nucifera* (NNU_XXXXX) genomes. A, Syntenic analysis of 6OMT and NMCH genes in the related species, *C. tomentella*, *A. coerulea*, and *M. cordata*. The green lines represented the anchored OMT genes; the red lines showed the NMCH genes in syntenic blocks. B, Syntenic analysis of NMCH genes between *C. tomentella* and *P. somniferum*. The red lines showed the NMCH genes in syntenic blocks. C, Maximum likelihood tree of NCS genes from candidate species. The red branches represented the NMCH genes localized in the syntenic blocks.

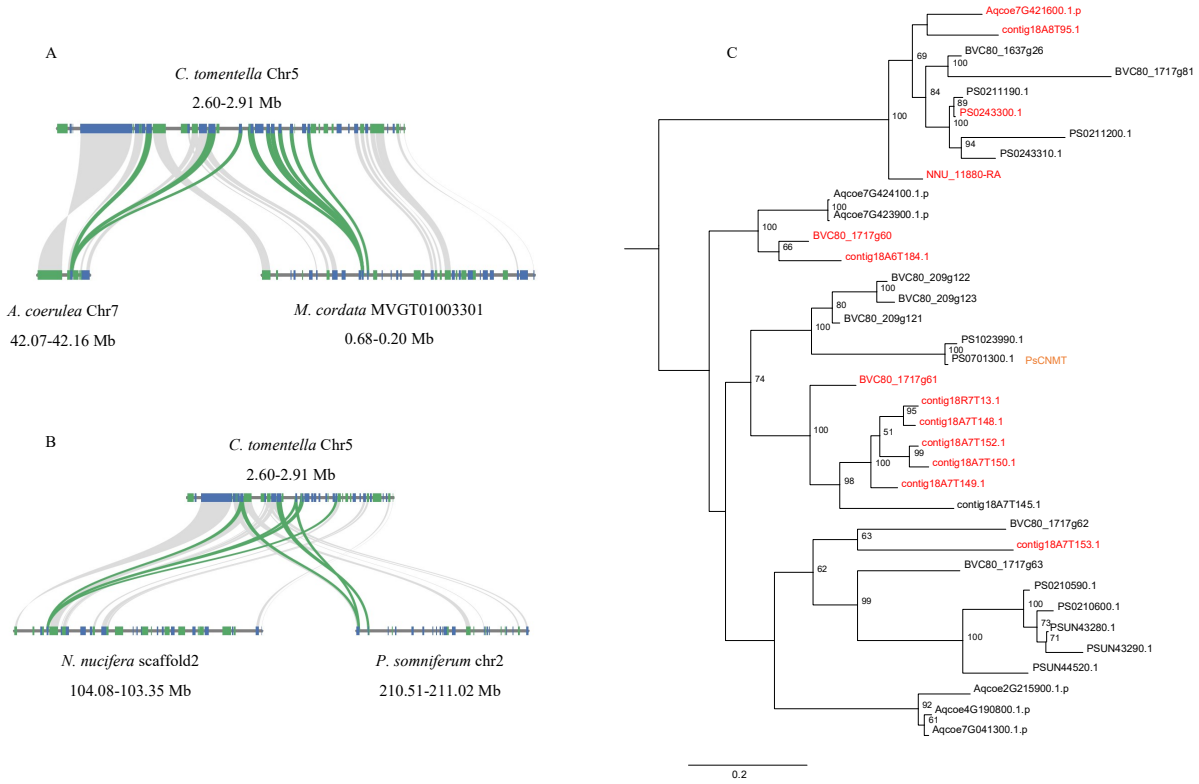

Figure S15. Evolutional analysis of NMT genes among *A. coerulea* (AqcoeXGXXXXXX), *C. tomentella* (contigXXXXXX), *M. cordata* (BVC80_XXXXXXX), *P. somniferum* (PSXXXXXXX), and *N. nucifera* (NNU_XXXXX) genomes. A, Syntenic analysis of NMT genes in the related species, *C. tomentella*, *A. coerulea*, and *M. cordata*. The green lines represented the anchored NMT genes. B, Syntenic analysis of NMT genes in the related species, *C. tomentella*, *N. nucifera*, and *P. somniferum*. The green lines represented the anchored NMT genes. C, Maximum likelihood tree of NMT genes from candidate species. The red branches represented the NMT genes localized in the syntenic blocks.

Figure S16. The classification of OMT genes identified from *A. coerulea* (AqcoeXGXXXXXX), *C. tomentella* (contigXXXXXX), *M. cordata* (BVC80_XXXXXXX), *P. somniferum* (PSXXXXXXX), and *N. nucifera* (NNU_XXXXX) genomes.

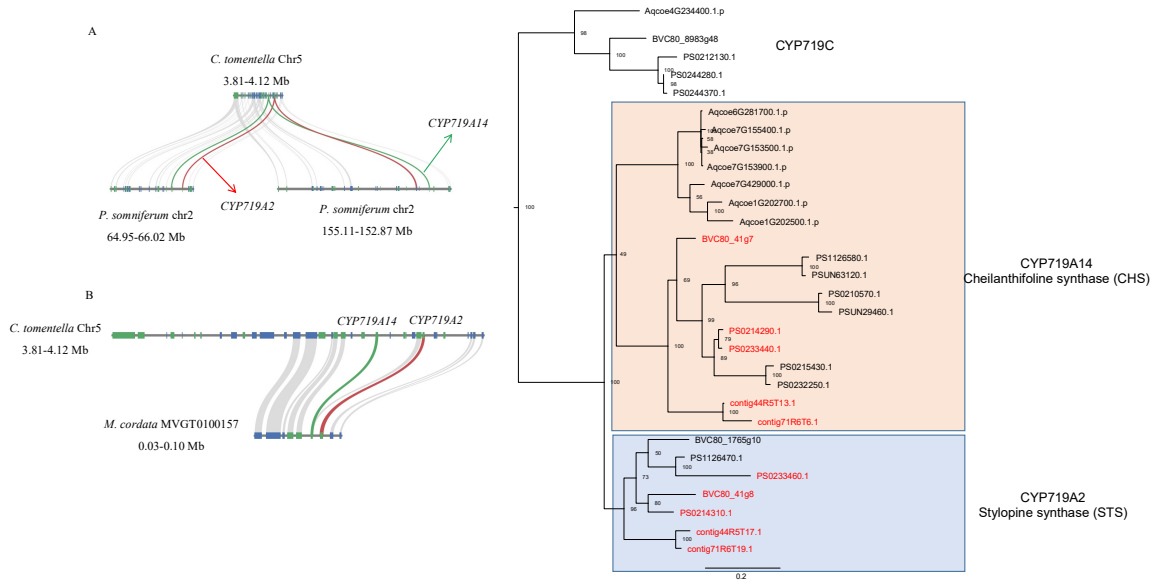

Figure S17. Evolutional analysis of CYP719 genes among the Papaveraceae species, *C. tomentella* (contigXXXXXX), *M. cordata* (BVC80_XXXXXXX), and *P. somniferum* (PSXXXXXXX). A, Syntenic analysis of CYP719 genes between *C. tomentella* and *P. somniferum*. The green lines represented the anchored CYP719A14 genes; the red lines represented the anchored CYP719A2 genes. B, Syntenic analysis of CYP719 genes between *C. tomentella* and *M. cordata*. The green lines represented the anchored CYP719A14 genes; the red lines represented the anchored CYP719A2 genes. C, Maximum likelihood tree of CYP719 genes from candidate species. The red branches represented the CYP719 genes localized in the syntenic blocks.

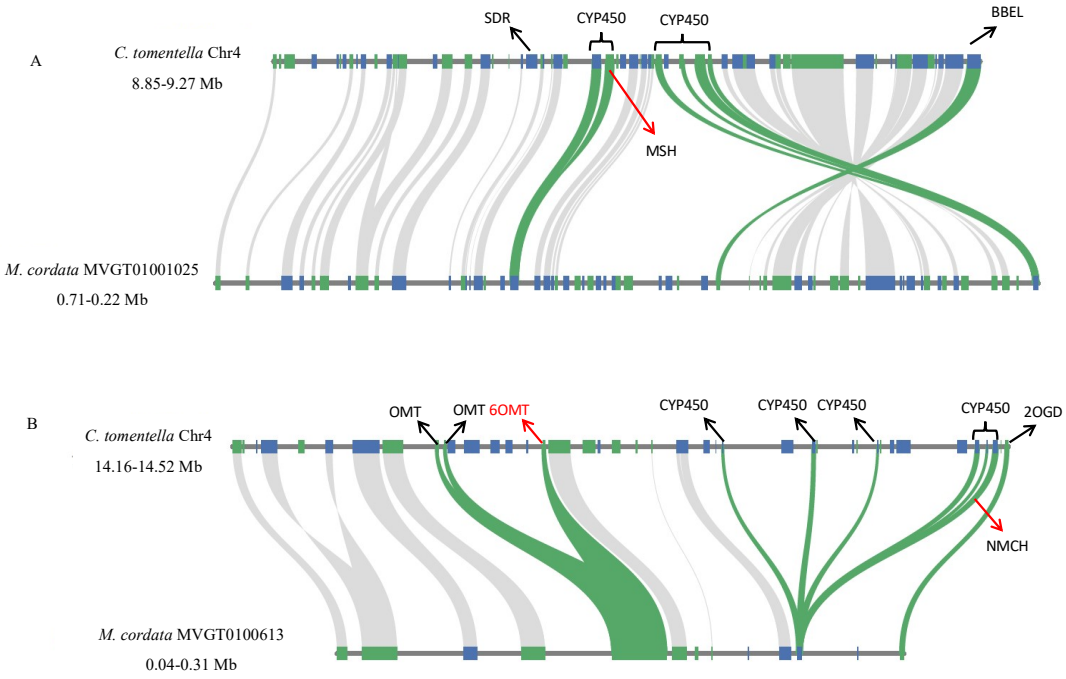

Figure S18. The collinearity analysis of conserved gene cluster related to the upstream biosynthesis of BIAs between *C. tomentella* and *M. cordata*. The arrows represented the related genes in BIA biosynthesis, including 6OMT, NMCH and MSH genes.

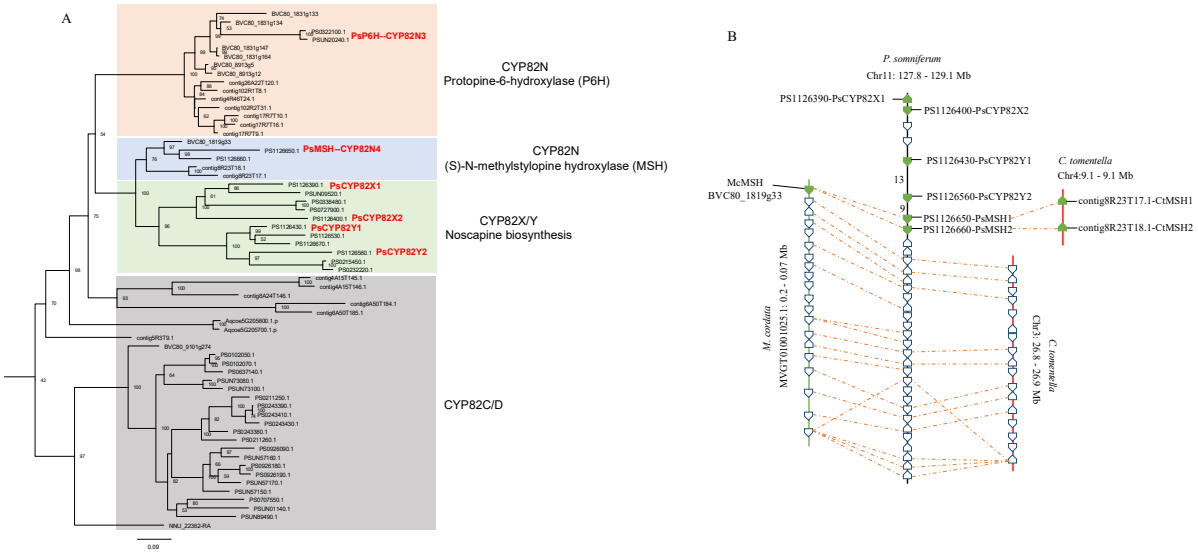

Figure S19. A, The classification of CYP82N, CYP82X, and CYP82Y subfamily members identified from *A. coerulea* (AqcoeXGXXXXXX), *C. tomentella* (contigXXXXXX), *M. cordata* (BVC80_XXXXXXX), *P. somniferum* (PSXXXXXXX), and *N. nucifera* (NNU_XXXXX) genomes. The red markers represented the functional gene in (S)-N-methylstylopine hydroxylase (MSH), (S)-protopine-6-hydroxylase (P6H) and related to noscapine biosynthesis. All of CYP82 genes identified from *A. coerulea* and *N. nucifera* genomes were classified into CYP82C/D subfamilies. B, The collinearity analysis of CYP82X/Y/N among *C. tomentella*, *M. cordata*, and *P. somniferum*. The green gene modules are CYP450 genes.

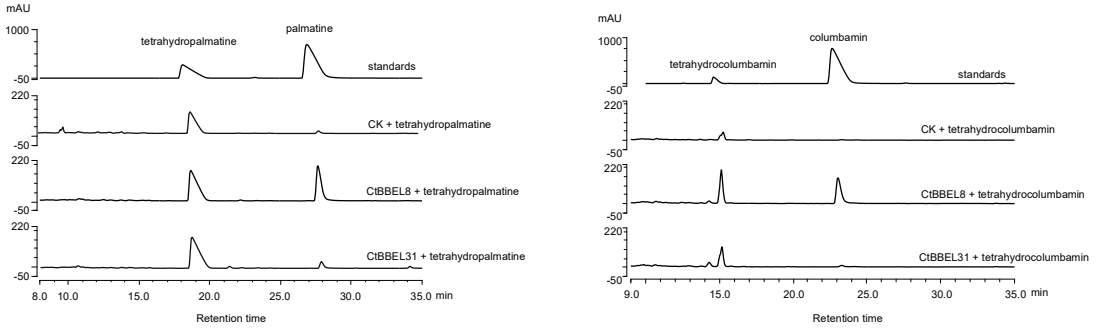

Figure S20. The *in vivo* catalytic assays of CtBBEL8 and CtBBEL31 in Sf9 insect cells using tetrahydrocolumbamin, and tetrahydropalmatine as substrates, respectively.

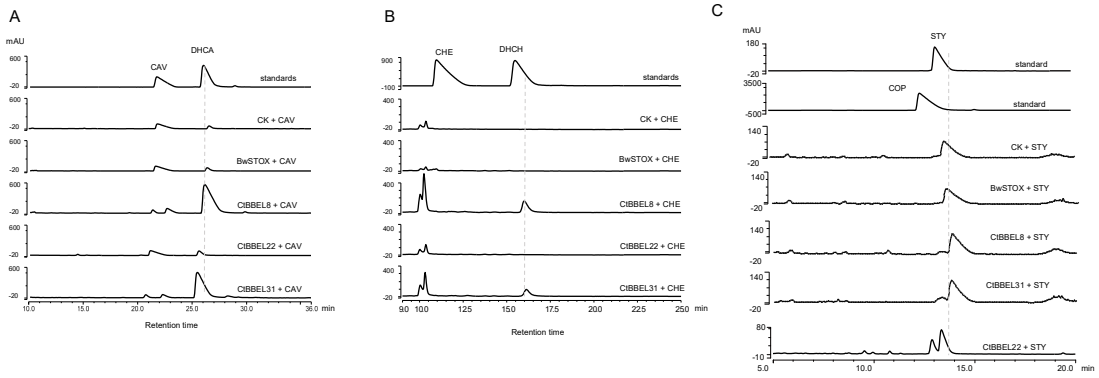

Figure S21. The *in vivo* catalytic assays of BwSTOX, CtBBEL8, CtBBEL22, and CtBBEL31 in Sf9 insect cells using cavidine (A), chilanthifoline (B), and stylopine (C) as substrates, respectively.

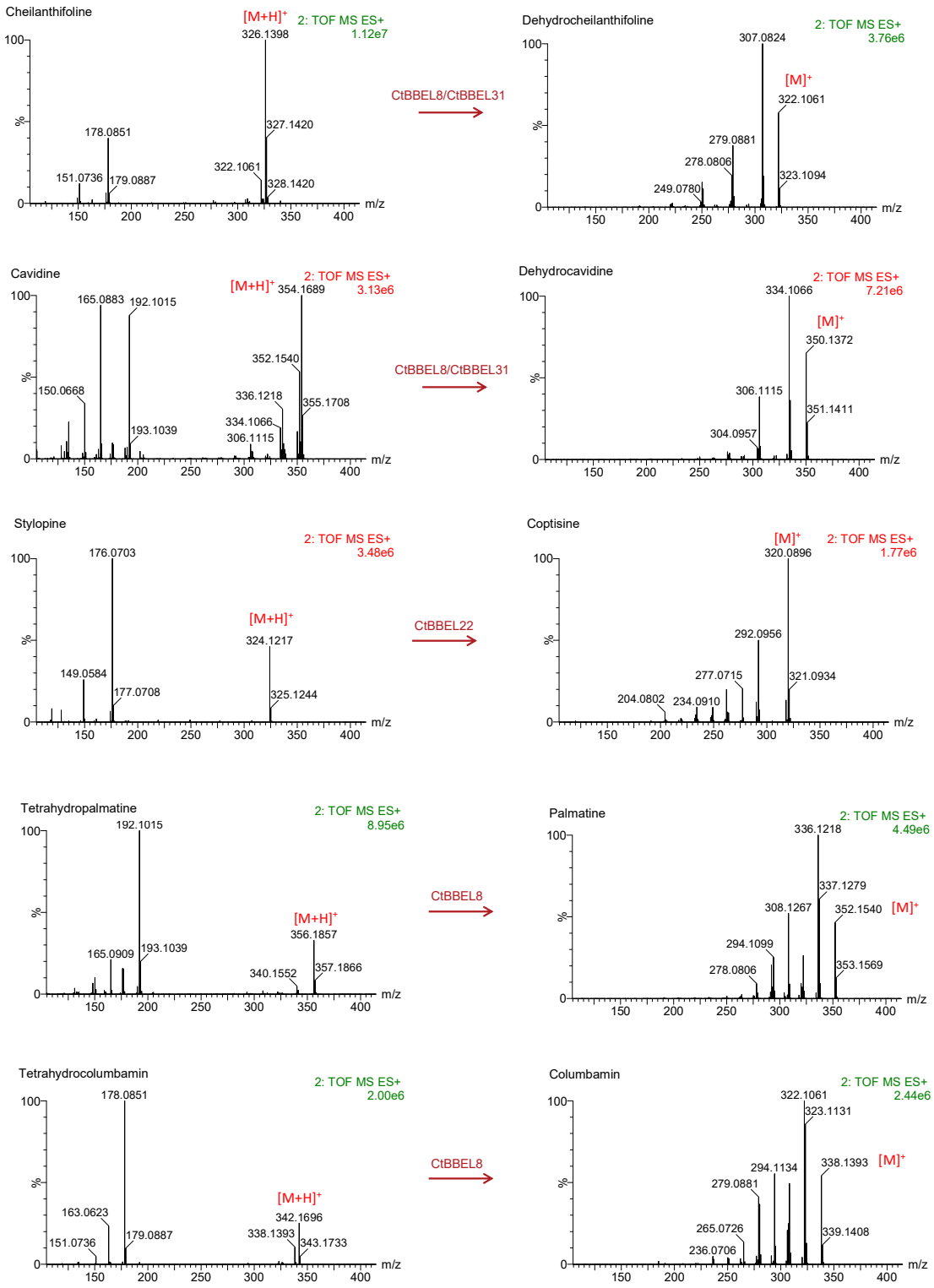

Figure S22. The LC-MS analysis of catalytic reaction of CtBBEL8, CtBBEL22, and CtBBEL31 using tetrahydrocolumbamin, tetrahydropalmatine, cheilanthifoline, cavidine, and stylopine as substrates, respectively.